PHYSICAL REVIEW A VOLUME 36, NUMBER 10 NOVEMBER 15, 1987

# Atomic collisions with relativistic heavy ions. IX. Ultrarelativistic collisions

R. Anholt* and U. Becker†
*Department of Physics, Stanford University, Stanford, California 94305-4060*
(Received 15 July 1987)

The behavior of projectile electron capture and ionization cross sections at ultrarelativistic energies ($>10$ GeV/amu) is discussed. Three mechanisms contribute to electron capture at these energies: radiative and nonradiative capture and the capture of the electron following electron-positron pair production. The radiative and nonradiative cross sections both fall off as $\gamma^{-1}$ at high energies, $(\gamma-1)Mc^2$ being the ion energy. The vacuum capture cross sections increase as the $\ln\gamma$. Projectile $1s$ ionization cross sections also increase as $\ln\gamma$ at high energies if target screening is negligible. However, when the projectile atomic number is smaller than the target atomic number, the transverse interaction giving the $\ln\gamma$ term is screened and reduced. Therefore, the total $1s$ ionization cross sections are dominated by Coulomb ionization, and are nearly constant with increasing projectile energy. Tables of reduced capture and ionization cross sections are given, and are applied to calculating the charge states of ions in matter and the lifetime of ions in storage rings.

## I. INTRODUCTION

This paper applies what we have learned about relativistic heavy-ion–atom collisions at energies below 2 GeV/amu (Refs. 1–5) to the consideration of ultrarelativistic collisions, where energies exceed 10 GeV/amu. At these high energies, the ion velocity is essentially the speed of light, and the relevant parameter describing the ion kinetic energy is $\gamma$, where the ion energy per nucleon is given by $(\gamma-1)Mc^2$, $M$ being the nucleon mass. We focus on processes affecting the charge states of relativistic ions in matter. Three electron-capture processes are considered: radiative (REC) (Ref. 1) and nonradiative (NRC) electron capture[6,7] and a process we call vacuum capture (VAC).[8,9] The former two processes have been discussed throughout this series of papers, and theories have been developed which accurately calculate the cross sections. For radiative capture cross sections, the impulse approximation is used, which relates the capture process to the inverse photoelectric process. For photoelectric cross sections at very high photon energies, corresponding to high projectile energies, the Sauter formula[10,11] give good agreement with data for low-$Z$ ions.[1] For nonradiative electron capture we have developed the eikonal approximation[6,7] to describe the capture from any filled shell of the target to any shell of the projectile.[2] Other theories have also been applied to our relativistic electron-capture data.[12–14] The vacuum-capture process is a new process, which has not been observed to date, because it comes into play at higher energies than we have had access to. Vacuum capture is a process where the target acts as a perturbing potential that excites an electron-positron pair in the field of the projectile nucleus. The positron is emitted and the electron is captured into the projectile $1s$ shell (and possibly into higher shells). The creation of an electron-positron pair is similar to the ionization process, except that momentum is imparted into the vacuum instead of into exciting an electron into a higher state. Electron-positron pairs are copiously emitted in relativistic heavy-ion–atom collisions. Vacuum capture is a less likely process, where the electron is captured into a shell of the projectile instead of being emitted. Like the ionization process at high energies, the vacuum-capture cross section depends on the square of the perturbing target nucleus charge, and increases as the $\ln\gamma$.

At relativistic energies, $1s$ ionization comes from three contributions:[5,15] a Coulomb part, which is the dominant part at nonrelativistic velocities, and approaches a constant when the projectile velocity approaches the speed of light; a transverse part, due to collisions at large impact parameters, and which increases as the $\ln\gamma^2$ at high velocities; and a spin-flip term, which also increases as $\ln\gamma$. When the perturbing target nucleus is screened, the transverse and spin-flip contributions coming from large impact parameters tend to be much more reduced by target-atom screening than the Coulomb part.[1] In this paper we show that when the projectile atomic number is smaller than the target atomic number, the transverse and spin-flip contributions to the ionization cross sections are negligible compared to the constant Coulomb part, hence low-$Z$ projectile $1s$ ionization cross sections are constant with increasing projectile energy.

At ultrarelativistic energies, the equilibrium charge state of all projectiles is fully stripped. Unless one is interested in measuring capture and loss for those projectiles having electron-bearing fractions less than $10^{-2}$, one need not perform elaborate calculations of projectile charge states. The present discussion is most relevant to the consideration of storing very-high-energy heavy ions in circulating storage rings.[16] There the lifetime of a fully stripped projectile can be limited by the magnitude of the electron-capture cross sections; once the projectile picks up an electron the ion is essentially lost in the next bending magnet.

Section II of this paper considers electron-capture

 

cross sections, and Sec. III projectile 1*s* ionization cross sections at ultrarelativistic energies. Tables of reduced capture and loss cross sections are presented. Examples of the use of these tables to calculate equilibrium charge states and storage-ring lifetimes are given in Sec. IV and the Appendix.

## II. ELECTRON CAPTURE

### A. Radiative electron capture

Radiative capture is the inverse of the photoelectric process, hence the REC cross sections can be calculated from 1*s* photoelectric cross sections. Paper II (Ref. 2) showed that for 1–2 GeV/amu light heavy ions of C, Ne, and Ar, the Sauter formula[10] with relativistic corrections of Pratt[11] gave good agreement with measurements. The Sauter formula is a high-velocity formula which is most valid when the velocity of the outgoing electron much exceeds the *K*-electron velocity ($\beta/Z\alpha \gg 1$), and the photon energy much exceeds the *K*-electron binding energy. For electron capture by $<1$-GeV/amu Xe and U ions,[2,4] we could not use the Sauter formula, since the photon energy was not sufficiently higher than the electron binding energy. However, for ultrarelativistic ions, where the photon energy exceeds several MeV, and where $\beta/Z\alpha > 1$, the Sauter formula with corrections should be adequate.

For large values of $\gamma$, the radiative capture cross section into the *K* shell of the projectile varies as

$$\sigma_{K_{\mathrm{REC}}} \sim Z_p^5 Z_t/\gamma \ , \tag{1}$$

where $Z_p$ is the projectile atomic number and $Z_t$ is the target atomic number. The factor of $Z_t$ comes from the fact that all target electrons have an equal probability of being captured, hence for the cross section per target atom, the cross section per electron is multiplied by the number of target electrons. Capture into *s* shells of the projectile is dominant. The cross section for capture into higher shells with quantum number *n* varies as $n^{-3}$, hence the total radiative capture cross section for bare projectiles is $\sim 1.2$ times the 1*s* capture cross section.

Figure 1 shows calculations of electron-capture cross sections multiplied by $\gamma$ versus $\gamma$. The cross sections approach the asymptotic limit, Eq. (1) at $\gamma = 15$. Table I gives reduced radiative electron capture cross sections, where the values at 100 GeV/amu have been multiplied by $\gamma/Z_p^5 Z_t$, to give slowly varying, easily interpolated cross sections. From this table, the radiative electron-capture cross section for any target-projectile combination at any $\gamma$ value exceeding 15 can be calculated with an error of less than 10%.

### B. Vacuum capture

The capture of an electron into the projectile 1*s* shell with the simultaneous emission of a positron has been calculated by Becker *et al.*[8] and by Bertulani and Baur.[9] Becker has compared calculations made in two different ways: using Dirac electron and positron wave functions where the interaction potential is expanded in a series of partial waves and using Sommerfeld-Maue wave functions[17] where the partial wave series is avoided. The

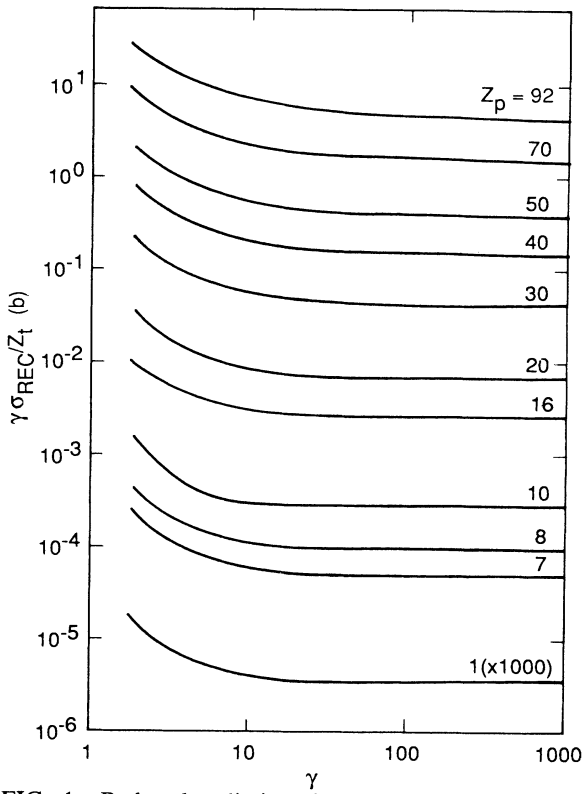


FIG. 1. Reduced radiative electron-capture cross sections plotted against $\gamma$ for various projectile atomic numbers.

Dirac wave functions are most accurate for heavy projectiles, but the partial wave series converges slowly for energies greater than 10 GeV/amu, so that even when up to 20 partial waves are included, the accuracy of the resulting cross sections is uncertain. The Sommerfeld-Maue wave functions are most accurate for low-*Z* projectiles, or for very high-velocity positrons. As for the Sauter formula for photoelectric cross sections, $\beta/Z\alpha$ should be much greater than unity for the application of these wave functions. In the cases tested, the Sommerfeld-Maue and Dirac wave functions gave identical results within 20% for all projectile atomic numbers and for $\gamma > 10$.

Figure 2 shows reduced vacuum-capture cross sections into the projectile *K* shell plotted against $\gamma$ for various projectiles. The vacuum-capture process involves a momentum-transfer step from the target nucleus to the vacuum followed by an electron-capture step into the projectile *K* shell. The vacuum-capture cross section therefore varies as the square of the perturbing charge, as for most momentum-transfer processes like ionization and excitation, and as $Z_p^5$, which is typical for projectile electron-capture processes. The excitation process mainly occurs through the transverse part of the perturbing interaction and, like transverse ionization, the cross section increases as $\ln\gamma$ for large $\gamma$ values. Unlike for ionization where the Coulomb part of the interaction gives a significant nonzero contribution to the total ionization cross section, the Coulomb part for vacuum capture is negligible, hence the vacuum cross sections vanish for $v \ll c$.

TABLE I. Reduced radiative and vacuum-capture cross sections.

| $Z_p$ | REC (nb) | VAC (pb) | $\gamma_0$ |
|---|---|---|---|
| 1 | 3.44 | 3.25 | 6.81 |
| 2 | 3.35 | 3.17 | 6.81 |
| 3 | 3.25 | 3.08 | 6.81 |
| 4 | 3.17 | 3.00 | 6.82 |
| 5 | 3.08 | 2.95 | 6.82 |
| 6 | 3.00 | 2.88 | 6.82 |
| 7 | 2.93 | 2.82 | 6.83 |
| 8 | 2.85 | 2.76 | 6.83 |
| 9 | 2.78 | 2.66 | 6.84 |
| 10 | 2.71 | 2.62 | 6.84 |
| 15 | 2.40 | 2.28 | 6.87 |
| 20 | 2.14 | 2.06 | 6.90 |
| 30 | 1.73 | 1.66 | 6.99 |
| 40 | 1.42 | 1.32 | 7.09 |
| 50 | 1.18 | 1.07 | 7.33 |
| 60 | 1.00 | 0.880 | 7.48 |
| 70 | 0.85 | 0.733 | 7.69 |
| 80 | 0.74 | 0.620 | 7.91 |
| 92 | 0.63 | 0.523 | 8.23 |

The curves shown in Fig. 2 have been fit with the expression

$$\sigma_{\mathrm{VAC}}=Z_p^5 Z_t^2 a \ln(\gamma/\gamma_0) , \tag{2}$$

where $a$ is a constant varying from 0.4 to 2.7 pb and $\gamma_0$ is the point where the straight part of the curves in Fig. 2 intercepts the $x$ axis. The values of $a$ and $\gamma_0$ are given in Table I. As capture into higher shells than the $K$ shell varies as $n^{-3}$, the value of $a$, calculated for $1s$ capture, was multiplied by 1.2 to include capture into all higher shells of the projectile. Equation (2) should only be used for $\gamma > \gamma_0$. It accurately describes the numerically calculated curves within approximately 20% when $\gamma > 10$.

Due to the high value of the momentum transfer needed to excite an electron-positron pair, vacuum capture takes place predominantly at small impact parameters, where the screening of the target nucleus by the target electrons is unimportant. However, an antiscreening term, due to the induced pair creation by the incident target electrons in the projectile frame can increase the probability of vacuum capture. This can be included by using $Z_t^2+Z_t$ in place of $Z_t$ in Eq. (2).

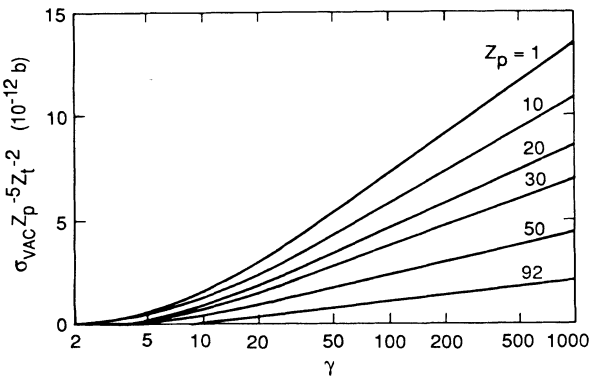


FIG. 2. Reduced vacuum-capture cross sections plotted against $\gamma$ for various projectile atomic numbers. For $\gamma > 10$, the cross sections on this semilog plot can be fitted to a straight line, with intercept near $\gamma = 7$.

### C. Nonradiative electron capture

This series of papers has focussed on the development of the eikonal approximation for nonradiative electron capture in relativistic heavy-ion collisions.[2,6,7] A simple formula for $1s$-$1s$ capture in the prior form of the asymmetric eikonal theory was proposed by Anholt and Eichler[6] and Eichler,[7] which was adapted to calculating total capture cross sections from any filled target shell to any projectile shell by scaling $Z_t$ and $Z_p$ by the principal quantum numbers $n$.[2] In addition, it was proposed to use the prior form if $Z_p/n_p < Z_t/n_t$ and otherwise the post form.[2] The post form is obtained from the prior form by interchanging $Z_p/n_p$ and $Z_t/n_t$. The scaling-law formula approximately agreed with experiment and with numerical calculations for both low-$Z$ and high-$Z$ ions. In general the agreement improved for higher-energy ions, hence we can confidently apply this prescription to the calculation of ultrarelativistic collisions.

In the case of very-high-energy ions, the nonradiative electron-capture cross section from any shell $n_t$ to any projectile shell with quantum number $n_p$ varies as[2]

$$\sigma_{\mathrm{NRC}} \sim \frac{Z_p^5 Z_t^5}{n_p^3 n_t^3 \gamma} , \tag{3}$$

hence the total capture cross section from any full occupied, high-$Z$ target into a bare projectile varies as

$$\sigma_{\mathrm{NRC}} \sim 1.4 Z_p^5 Z_t^5/\gamma . \tag{4}$$

In Fig. 3 we show reduced NRC cross sections versus $\gamma$ for $S$ projectile and for target atomic numbers between 1 and 92. In general, for all $Z_t > 10$ and for all $\gamma > 30$, the reduced NRC cross sections, $\sigma_{\mathrm{NRC}}\gamma/(Z_p Z_t)^5$ are constant and equal to about $8\times10^{-18}$ b. For $\gamma < 30$ the cross sections fall off faster than $\gamma^{-1}$, hence the asymptotic reduced cross sections cannot be used for those energies. Table II gives reduced cross sections for any $Z_t$ and any $Z_p$ value. The cross sections were calculated for $\gamma = 100$, but the reduced cross sections can be calculated from Table II with an accuracy of less than 20% for any $\gamma > 40$. Dividing the cross sections by $(Z_p Z_t)^5$ clearly removes most of the dependences on $Z_p$ and $Z_t$, though some residual dependence remains, possibly due to relativistic-electron wave-function effects at high $Z$, or to post-prior discrepancies and occupation factors at low $Z$.

## III. $1s$ IONIZATION CROSS SECTIONS

We have previously considered the case of target $K$-shell ionization by relativistic projectiles.[5] Simple formulas were derived, and were compared with data for $\gamma$ as large as 2000 (900-MeV electron induced $K$-shell ion-

TABLE II. Reduced nonradiative electron-capture cross sections ($10^{-18}$ b).

| $Z_p$ \ $Z_t$ | 1 | 2 | 4 | 7 | 10 | 13 | 18 | 29 | 36 | 47 | 54 | 73 | 92 |
|---|---|---|---|---|---|---|---|---|---|---|---|---|---|
| 1 | 2.21 | 5.69 | 8.16 | 8.96 | 8.98 | 8.75 | 8.18 | 6.96 | 6.37 | 5.73 | 5.47 | 5.24 | 5.63 |
| 2 | 2.15 | 5.69 | 8.23 | 9.03 | 9.05 | 8.82 | 8.25 | 7.02 | 6.42 | 5.77 | 5.51 | 5.27 | 5.66 |
| 4 | 2.04 | 5.42 | 8.28 | 9.17 | 9.20 | 8.97 | 8.39 | 7.14 | 6.53 | 5.86 | 5.59 | 5.33 | 5.70 |
| 5 | 1.98 | 5.28 | 8.09 | 9.24 | 9.26 | 9.04 | 8.46 | 7.20 | 6.58 | 5.90 | 5.63 | 5.36 | 5.73 |
| 6 | 1.93 | 5.14 | 7.91 | 9.30 | 9.32 | 9.10 | 8.53 | 7.26 | 6.63 | 5.95 | 5.67 | 5.39 | 5.75 |
| 7 | 1.88 | 5.01 | 7.74 | 9.29 | 9.38 | 9.15 | 8.59 | 7.31 | 6.69 | 5.99 | 5.71 | 5.42 | 5.77 |
| 8 | 1.83 | 4.88 | 7.56 | 9.09 | 9.45 | 9.21 | 8.65 | 7.37 | 6.74 | 6.04 | 5.75 | 5.45 | 5.80 |
| 9 | 1.79 | 4.76 | 7.38 | 8.89 | 9.51 | 9.26 | 8.70 | 7.43 | 6.79 | 6.08 | 5.79 | 5.47 | 5.82 |
| 10 | 1.74 | 4.65 | 7.21 | 8.71 | 9.49 | 9.32 | 8.74 | 7.49 | 6.84 | 6.12 | 5.83 | 5.50 | 5.84 |
| 15 | 1.55 | 4.13 | 6.42 | 7.86 | 8.59 | 9.05 | 8.97 | 7.71 | 7.09 | 6.33 | 6.02 | 5.65 | 5.96 |
| 20 | 1.39 | 3.71 | 5.77 | 7.10 | 7.85 | 8.26 | 8.73 | 7.86 | 7.24 | 6.53 | 6.19 | 5.80 | 6.07 |
| 25 | 1.26 | 3.37 | 5.24 | 6.45 | 7.15 | 7.63 | 8.03 | 8.04 | 7.36 | 6.65 | 6.37 | 5.92 | 6.19 |
| 30 | 1.16 | 3.09 | 4.81 | 5.92 | 6.58 | 7.03 | 7.47 | 8.01 | 7.50 | 6.73 | 6.43 | 6.04 | 6.28 |
| 40 | 1.01 | 2.69 | 4.18 | 5.14 | 5.71 | 6.13 | 6.60 | 7.06 | 7.28 | 6.95 | 6.59 | 6.19 | 6.47 |
| 50 | 0.92 | 2.44 | 3.78 | 4.63 | 5.14 | 5.51 | 5.96 | 6.47 | 6.63 | 6.90 | 6.80 | 6.29 | 6.57 |
| 60 | 0.86 | 2.29 | 3.55 | 4.33 | 4.79 | 5.13 | 5.54 | 6.11 | 6.25 | 6.44 | 6.59 | 6.43 | 6.64 |
| 70 | 0.84 | 2.22 | 3.44 | 4.19 | 4.62 | 4.93 | 5.32 | 5.85 | 6.08 | 6.21 | 6.32 | 6.60 | 6.75 |
| 80 | 0.84 | 2.23 | 3.44 | 4.19 | 4.60 | 4.90 | 5.26 | 5.78 | 6.00 | 6.19 | 6.27 | 6.58 | 6.89 |
| 92 | 0.88 | 2.35 | 3.61 | 4.38 | 4.80 | 5.09 | 5.44 | 5.96 | 6.17 | 6.44 | 6.50 | 6.74 | 7.09 |

ization). Here we consider projectile ionization. As for target ionization, the cross section can be written as the sum of three contributions due to Coulomb ionization, transverse ionization, and ionization involving the spin-flip of the ionized electron.[5] The Coulomb-ionization cross section is the same as that calculated using the plane-wave-Born approximation for nonrelativistic projectiles. The cross sections can be obtained from tables[18-19] of the function $f(\eta_K)$ using

$$\sigma_{\text{Coul}}=\frac{4\pi a_0^2 Z_t^2}{\eta_K Z_p^4} f(\eta_K) , \tag{5}$$

where for the present projectile ionization cross sections

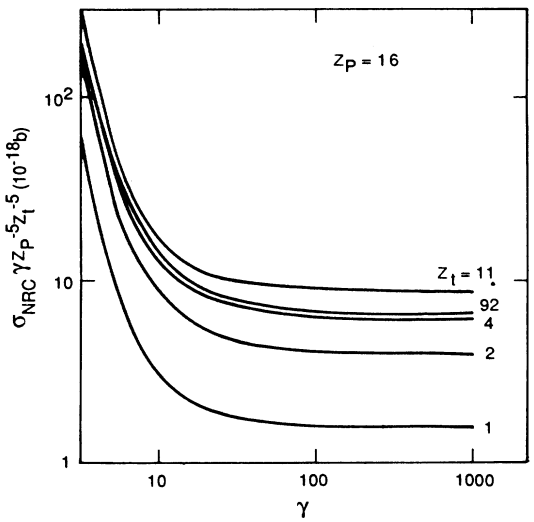


FIG. 3. Reduced nonradiative electron-capture cross sections for $S$ ions plotted against $\gamma$ for various target atomic numbers.

the target and projectile atomic numbers are reversed from the normal convention, and the cross section is defined per electron, not per atom, hence is a factor of 0.5 smaller. For relativistic projectiles, $\eta_K$ is given by

$$\eta_K=(\beta/Z_p\alpha)^2 . \tag{6}$$

For ultrarelativistic projectiles, $\beta=1$ and the cross section can be written as

$$\sigma_{\text{Coul}}=1.87\times10^4(Z_t/Z_p)^2 f((Z_p\alpha)^{-2}) \text{ b electron} , \tag{7}$$

for large $\gamma$, $\sigma_{\text{Coul}}$ is independent of the ion energy. The factor $Z_t^2$ is due to the strength of the perturbing Coulomb interaction between the target nucleus and projectile electron. The factor $Z_p^{-2}$ reflects the variation of the cross section with the a real size of the projectile $K$ shell. We can derive a reduced cross section, by multiplying $\sigma_{\text{Coul}}$ by $Z_p^2/Z_t^2$,

$$\sigma_{\text{Coul}}(Z_p/Z_t)^2=1.87\times10^4 f((Z_p\alpha)^{-2}) , \tag{8}$$

which should vary only slowly with $Z_p$, as $f(\eta)$ varies logarithmically with $\eta$.

The second contribution to $1s$ ionization comes from the transverse interaction between the target nucleus and projectile electron. This interaction is most important in collisions with large impact parameters. For most relevant $\gamma$ values, the transverse projectile ionization cross section can be written as[5]

$$\sigma_{\text{trans}}(Z_p/Z_t)^2=0.523\times10^4\frac{\ln\gamma^2-\beta^2}{\beta^2} \text{ b/electron} . \tag{9}$$

This can be deduced from Eq. (24) of Ref. 5 for target ionization by setting $\theta_K=1$, setting $Z_1=Z_t$ and $Z_2=Z_p$ for projectile ionization, and dividing the cross section per atom by 2.

The last contribution to $K$-shell ionization comes from

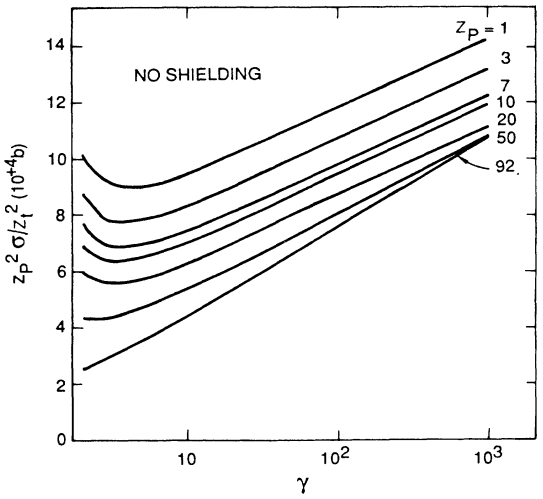


FIG. 4. Reduced ionization cross sections for various projectiles plotted against $\gamma$. No target screening is included in these calculations, hence the reduced cross sections are independent of $Z_t$.

the spin-flip interaction, which is part of the transverse interaction, and which also increases as the $\ln\gamma$ at high velocities. Being a higher-order contribution, the relative strength of the interaction depends on $Z_p\alpha$, hence this term is most important for $U$ projectile ionization.

Figure 4 shows reduced total ionization cross sections for several projectiles incident on bare target ions. For $\gamma < 3$, the cross sections fall off with increasing $\gamma$. This is due to the $\eta_K^{-1}$ dependence of the Coulomb ionization cross sections, which fall off then approach a constant, when the velocity approached the speed of light. The magnitudes of the reduced ionization cross sections decrease with increasing $Z_p$. This is due to the logarithmic dependence of the Coulomb part of the cross sections on $\eta_K$ or $Z_p\alpha$. For all $Z_p < 50$, the cross sections increase as $\ln\gamma$ above $\gamma = 10$, due to the transverse interaction. The spin-flip contribution increases the slope of the cross sections for $Z_p > 50$.

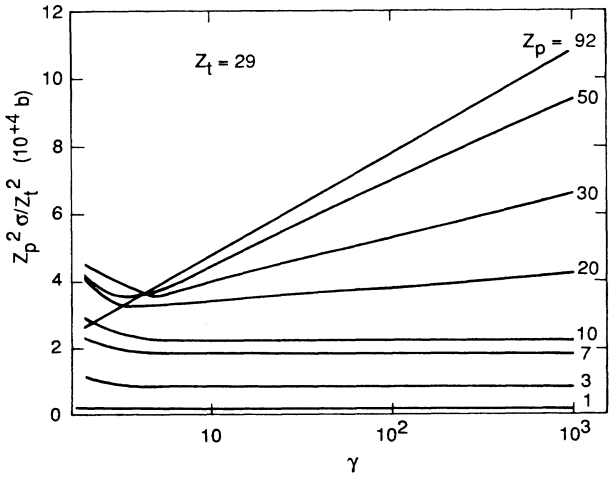


FIG. 5. Same as Fig. 4 for excitation by screened Cu target atoms.

Figure 5 shows reduced cross sections for projectile ionization by Cu atoms. The screened plane-wave-Born approximation cross sections were calculated using the screening plus antiscreening function $S(q')$, described in paper II (Ref. 1) and elsewhere.[3,4,20] Unlike in previous papers, however, we have modified $q'$ to take into account the retardation of the target screening potential in the projectile frame by setting $q'^2 = q^2 - q_0^2\beta^2$, where $q$ is momentum transfer and $q_0$ is the minimum momentum transfer needed to ionize the projectile $1s$ electron. This substitution has no effect on the cross sections previously calculated where $\gamma < 3$. For $\gamma = 100$, the substitution at most reduces some transverse cross sections by a factor of 0.5. Since the transverse cross sections come from larger impact parameters, where the projectile electron tends to see a nearly neutral perturbing atom, the transverse and spin-flip contributions to the total ionization cross sections are much reduced at large $\gamma$ values, below that calculated without screening. For $Z_p < Z_t$, the total ionization cross sections are smaller than the unscreened ones, and are constant with $\gamma$, indicating that the transverse cross sections are virtually eliminated. However, for $Z_p \gg Z_t$, the impact parameters contributing to both Coulomb and transverse ionization are so small compared to the average distances of the target electrons from the target nucleus that the projectile electron always sees an unscreened perturbing nucleus. The screened cross sections for U ionization in Fig. 5 are nearly equal to the unscreened ones in Fig. 4.

To calculate total projectile ionization cross sections for any value of $Z_t$ and $Z_p$ we present reduced Coulomb and transverse plus spin-flip cross sections in Tables III and IV. In terms of these reduced values, the total ionization cross section is given by

$$\sigma_{\text{tot}} = \sigma_{\text{Coul}} + \sigma_{\text{trans}} ,$$

$$\sigma_{\text{Coul}} = s(Z_t, Z_p) \times 10^4 \left[ \frac{Z_t}{Z_p} \right]^2 \text{ b/electron} , \tag{10}$$

$$\sigma_{\text{trans}} = t(Z_t, Z_p) \times 10^4 \left[ \frac{Z_t}{Z_p} \right]^2 \frac{\ln\gamma^2 - \beta^2}{\beta^2} \text{ b/electron} ,$$

where $s$ is in Table III and $t$ in Table IV. For constant $Z_t$, the values of $s$ depend logarithmically on $Z_p$. For reference, the unscreened $s$ and $t$ values are given in the column denoted by $Z_t = 0$ in Tables III and IV. For $Z_t = 0$, $t$ is constant for $Z_p < 50$ but increases for large $Z_p$, due to the spin-flip contribution. For constant $Z_p$ when $Z_p \gg Z_t$, $s$ and $t$ are close to the unscreened values at high $Z_t$ and are twice the unscreened values at $Z_t = 1$. The factor-of-2 increase for H-atom excitation is due to antiscreening; the projectile electron can be excited with equal probability by the projectile nucleus or by the H-atom's electron. For constant $Z_p < Z_t$, the reduced $s$ and $t$ values decrease with increasing $Z_t$ due to the screening effect. Note that the $s$ values are as small as one to two orders of magnitude below the unscreened values, but the transverse $t$ values are over six orders of magnitude smaller.

TABLE III. Reduced Coulomb ionization cross sections ($10^4$ b).

| $Z_p$ \ $Z_t$ | 0 | 1 | 2 | 4 | 7 | 10 | 13 | 18 | 29 | 36 | 47 | 54 | 73 | 92 |
|---|---|---|---|---|---|---|---|---|---|---|---|---|---|---|
| 1 | 7.53 | 2.37 | 0.84 | 0.91 | 0.53 | 0.30 | 0.33 | 0.29 | 0.18 | 0.17 | 0.15 | 0.15 | 0.11 | 0.11 |
| 2 | 6.80 | 4.21 | 1.87 | 1.63 | 1.19 | 0.82 | 0.77 | 0.71 | 0.52 | 0.47 | 0.44 | 0.43 | 0.34 | 0.32 |
| 3 | 6.37 | 5.33 | 2.66 | 2.14 | 1.67 | 1.28 | 1.16 | 1.07 | 0.85 | 0.77 | 0.72 | 0.70 | 0.58 | 0.55 |
| 4 | 6.06 | 6.08 | 3.25 | 2.53 | 2.04 | 1.64 | 1.49 | 1.36 | 1.14 | 1.04 | 0.97 | 0.94 | 0.81 | 0.76 |
| 5 | 5.82 | 6.61 | 3.71 | 2.86 | 2.32 | 1.93 | 1.77 | 1.61 | 1.38 | 1.27 | 1.18 | 1.15 | 1.02 | 0.95 |
| 6 | 5.62 | 7.02 | 4.07 | 3.12 | 2.56 | 2.17 | 2.01 | 1.83 | 1.59 | 1.48 | 1.38 | 1.34 | 1.20 | 1.13 |
| 7 | 5.46 | 7.33 | 4.36 | 3.35 | 2.76 | 2.37 | 2.20 | 2.02 | 1.77 | 1.66 | 1.55 | 1.51 | 1.37 | 1.28 |
| 8 | 5.31 | 7.56 | 4.60 | 3.53 | 2.92 | 2.54 | 2.37 | 2.18 | 1.93 | 1.81 | 1.70 | 1.65 | 1.51 | 1.43 |
| 9 | 5.19 | 7.75 | 4.79 | 3.69 | 3.07 | 2.69 | 2.52 | 2.33 | 2.06 | 1.95 | 1.83 | 1.79 | 1.65 | 1.56 |
| 10 | 5.07 | 7.89 | 4.95 | 3.82 | 3.19 | 2.81 | 2.64 | 2.45 | 2.19 | 2.07 | 1.96 | 1.90 | 1.76 | 1.67 |
| 15 | 4.62 | 8.15 | 5.41 | 4.20 | 3.59 | 3.23 | 3.05 | 2.87 | 2.62 | 2.51 | 2.39 | 2.34 | 2.20 | 2.11 |
| 20 | 4.28 | 8.01 | 5.52 | 4.31 | 3.74 | 3.43 | 3.25 | 3.08 | 2.85 | 2.75 | 2.64 | 2.59 | 2.46 | 2.37 |
| 30 | 3.77 | 7.38 | 5.31 | 4.22 | 3.72 | 3.48 | 3.33 | 3.17 | 2.99 | 2.91 | 2.82 | 2.77 | 2.67 | 2.60 |
| 40 | 3.36 | 6.67 | 4.90 | 3.95 | 3.51 | 3.31 | 3.19 | 3.06 | 2.91 | 2.85 | 2.78 | 2.74 | 2.66 | 2.60 |
| 50 | 2.99 | 5.96 | 4.43 | 3.61 | 3.23 | 3.06 | 2.95 | 2.85 | 2.73 | 2.68 | 2.62 | 2.59 | 2.53 | 2.48 |
| 60 | 2.65 | 5.30 | 3.95 | 3.24 | 2.92 | 2.77 | 2.69 | 2.60 | 2.50 | 2.45 | 2.41 | 2.39 | 2.34 | 2.30 |
| 70 | 2.34 | 4.67 | 3.50 | 2.88 | 2.60 | 2.48 | 2.41 | 2.33 | 2.24 | 2.21 | 2.17 | 2.16 | 2.12 | 2.09 |
| 80 | 2.04 | 4.08 | 3.06 | 2.53 | 2.29 | 2.19 | 2.13 | 2.06 | 1.99 | 1.96 | 1.93 | 1.92 | 1.89 | 1.86 |
| 92 | 1.72 | 3.43 | 2.57 | 2.14 | 1.93 | 1.85 | 1.80 | 1.75 | 1.69 | 1.67 | 1.65 | 1.64 | 1.61 | 1.59 |

The use of Eq. (9) is most accurate for $\gamma > 4$. For accurate Coulomb-ionization cross sections the ion velocity must be close to the speed of light, which is adequately satisfied for $\gamma > 4$. The transverse cross sections are negligible compared with the longitudinal ones for $\gamma < 4$, so the accuracy of Eq. (9) for transverse excitation at low $\gamma$ is immaterial.

## IV. APPLICATIONS

Tables I–IV can be used to calculate the total capture and ionization cross sections for any projectile-target combination, and for any energy. For ions in gas targets, the equilibrium fraction of projectiles carrying an electron is given by the ratio of the total capture cross section to the total ionization cross section[1]

$$R_{\rm eq} = \frac{\sigma_{\rm capt}}{\sigma_{\rm ioniz}} . \tag{11}$$

Figure 6 shows calculated cross sections and equilibrium ratios for a variety of 100-GeV/amu projectiles incident on targets with atomic number $Z_t$. The ionization cross

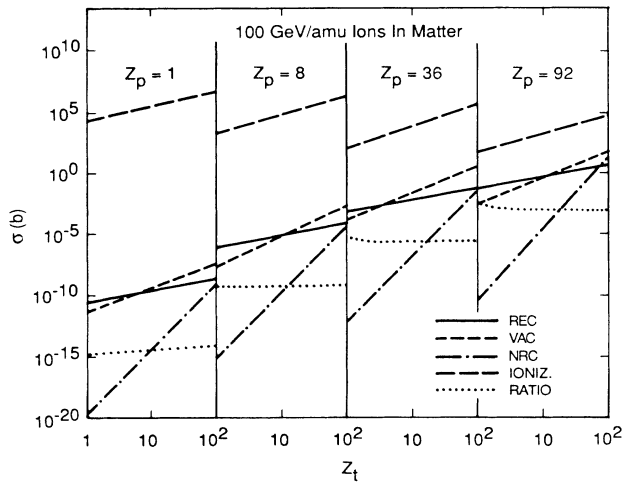


FIG. 6. 1s ionization, radiative (REC), nonradiative (NRC), and vacuum-capture (VAC) cross sections for 100-GeV/amu H, O, Kr, and U projectiles plotted against $Z_t$. The equilibrium fraction of electron-bearing projectiles in gas targets is shown by the dotted line.

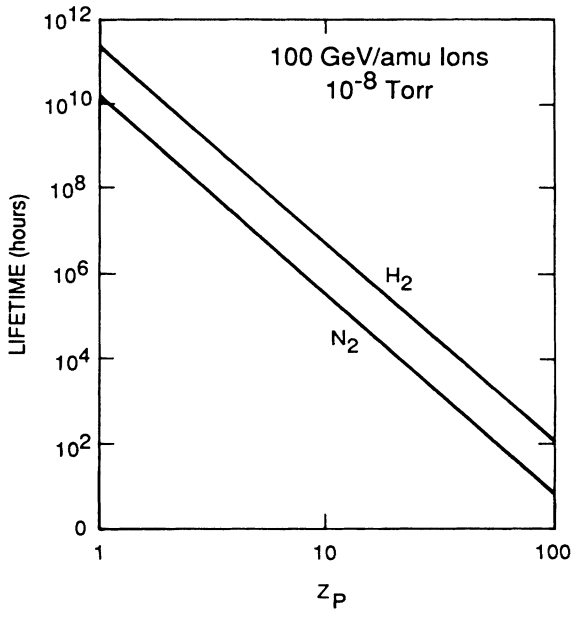


FIG. 7. Lifetime of stored 100-GeV/amu ions in storage rings with a vacuum of $10^{-8}$ torr plotted against projectile atomic number. This calculation assumes that the limiting process for ion loss from the ring is due to electron capture by the bare projectiles.

TABLE IV. Reduced transverse ionization cross sections ($10^{-4}$ b).

| $Z_p$ \ $Z_t$ | 0 | 1 | 2 | 4 | 7 | 10 | 13 | 18 | 29 | 36 | 47 | 54 | 73 | 92 |
|---|---|---|---|---|---|---|---|---|---|---|---|---|---|---|
| 1 | 5.26(−1) | 5.03(−5) | 1.60(−5) | 1.81(−5) | 1.49(−5) | 4.98(−6) | 6.59(−6) | 5.66(−6) | 3.78(−6) | 2.55(−6) | 2.24(−6) | 2.07(−6) | 2.08(−6) | 1.74(−6) |
| 2 | 5.27(−1) | 3.40(−4) | 1.07(−4) | 1.27(−4) | 8.05(−5) | 3.59(−5) | 4.61(−5) | 3.67(−5) | 2.59(−5) | 2.11(−5) | 1.89(−5) | 1.80(−5) | 1.68(−5) | 1.52(−5) |
| 3 | 5.27(−1) | 1.16(−3) | 3.51(−4) | 4.39(−4) | 2.35(−4) | 1.17(−4) | 1.52(−4) | 1.15(−4) | 8.15(−5) | 7.09(−5) | 6.40(−5) | 6.25(−5) | 5.55(−5) | 5.22(−5) |
| 4 | 5.27(−1) | 2.84(−3) | 8.39(−4) | 1.08(−3) | 5.28(−4) | 2.76(−4) | 3.63(−4) | 2.69(−4) | 1.87(−4) | 1.69(−4) | 1.53(−4) | 1.51(−4) | 1.30(−4) | 1.25(−4) |
| 5 | 5.28(−1) | 5.74(−3) | 1.67(−3) | 2.20(−3) | 1.01(−3) | 5.47(−4) | 7.20(−4) | 5.27(−4) | 3.62(−4) | 3.34(−4) | 3.02(−4) | 3.01(−4) | 2.53(−4) | 2.47(−4) |
| 6 | 5.28(−1) | 1.02(−2) | 2.95(−3) | 3.89(−3) | 1.74(−3) | 9.63(−4) | 1.27(−3) | 9.24(−4) | 6.25(−4) | 5.86(−4) | 5.30(−4) | 5.31(−4) | 4.39(−4) | 4.31(−4) |
| 7 | 5.28(−1) | 1.63(−2) | 4.76(−3) | 6.26(−3) | 2.78(−3) | 1.56(−3) | 2.04(−3) | 1.49(−3) | 9.99(−4) | 9.45(−4) | 8.55(−4) | 8.59(−4) | 7.00(−4) | 6.92(−4) |
| 8 | 5.29(−1) | 2.44(−2) | 7.18(−3) | 9.38(−3) | 4.17(−3) | 2.36(−3) | 3.07(−3) | 2.27(−3) | 1.50(−3) | 1.43(−3) | 1.29(−3) | 1.30(−3) | 1.05(−3) | 1.04(−3) |
| 9 | 5.29(−1) | 3.46(−2) | 1.03(−2) | 1.33(−2) | 5.98(−3) | 3.41(−3) | 4.39(−3) | 3.28(−3) | 2.16(−3) | 2.06(−3) | 1.87(−3) | 1.88(−3) | 1.51(−3) | 1.50(−3) |
| 10 | 5.30(−1) | 4.70(−2) | 1.41(−2) | 1.81(−2) | 8.26(−3) | 4.73(−3) | 6.03(−3) | 4.55(−3) | 3.00(−3) | 2.86(−3) | 2.59(−3) | 2.61(−3) | 2.09(−3) | 2.07(−3) |
| 15 | 5.32(−1) | 1.45(−1) | 4.61(−2) | 5.67(−2) | 2.77(−2) | 1.63(−2) | 2.00(−2) | 1.58(−2) | 1.04(−2) | 9.87(−3) | 8.97(−3) | 9.04(−3) | 7.21(−3) | 7.14(−3) |
| 20 | 0.54 | 0.30 | 0.10 | 0.12 | 0.06 | 0.04 | 0.05 | 0.04 | 0.02 | 0.02 | 0.02 | 0.02 | 0.02 | 0.02 |
| 30 | 0.54 | 0.68 | 0.28 | 0.27 | 0.19 | 0.12 | 0.12 | 0.11 | 0.08 | 0.08 | 0.07 | 0.07 | 0.06 | 0.05 |
| 40 | 0.58 | 1.00 | 0.53 | 0.41 | 0.35 | 0.27 | 0.24 | 0.24 | 0.19 | 0.17 | 0.17 | 0.16 | 0.14 | 0.13 |
| 50 | 0.60 | 1.16 | 0.74 | 0.51 | 0.47 | 0.42 | 0.36 | 0.34 | 0.31 | 0.28 | 0.27 | 0.26 | 0.23 | 0.22 |
| 60 | 0.63 | 1.25 | 0.87 | 0.62 | 0.55 | 0.52 | 0.48 | 0.43 | 0.41 | 0.38 | 0.36 | 0.35 | 0.33 | 0.31 |
| 70 | 0.66 | 1.32 | 0.96 | 0.72 | 0.62 | 0.60 | 0.57 | 0.52 | 0.49 | 0.48 | 0.44 | 0.43 | 0.42 | 0.40 |
| 80 | 0.69 | 1.37 | 1.02 | 0.80 | 0.68 | 0.65 | 0.63 | 0.60 | 0.56 | 0.55 | 0.52 | 0.51 | 0.50 | 0.47 |
| 92 | 0.71 | 1.43 | 1.07 | 0.86 | 0.75 | 0.70 | 0.69 | 0.66 | 0.62 | 0.61 | 0.60 | 0.58 | 0.56 | 0.55 |

sections far exceed the capture cross sections, hence $R_{eq} \ll 1$; the ions are nearly always fully stripped. The ionization cross sections increase almost with the square of $Z_t$, and fall off as $Z_p^{-2}$ for constant $Z_t$. The REC, VAC, and NRC capture cross sections increase as $Z_t$, $Z_t^2$, and $Z_t^5$. At low $Z_t$ REC is always dominant, but at high $Z_t$ vacuum capture is dominant. The equilibrium ratio increases slightly with $Z_t$ at low $Z_p$, due to the fact that the ionization cross sections do not increase as the square of $Z_t$, but the dominant vacuum-capture cross sections do. At high $Z_p$, $R_{eq}$ at first falls, when REC is dominant, then approaches a constant when VAC is dominant.

If a fully stripped ion circulating in a storage ring captures an electron, the projectile will be misbent by subsequent steering magnets, resulting in the loss of the ion from the ring. Figure 7 shows a calculation of the lifetime of stored heavy ions limited by electron capture for a vacuum of $10^{-8}$ torr of air (modeled by $N_2$), or $H_2$ (which is the dominant residual gas in cryopumped storage rings). The lifetime is proportional to the inverse of the product of the capture cross section and the target pressure (Appendix A). REC is dominant for the relevant low target atomic numbers, hence the capture cross sections are proportional to $Z_p^5$, and the lifetime falls off by ten orders of magnitude as $Z_p$ increases two orders of magnitude in Fig. 7. For larger ion energies the lifetime increases linearly with $\gamma$. Clearly, for ions with $Z_p < 50$, electron capture does not affect the storage lifetimes significantly. In fact, the capture cross sections are usually much smaller than typical 100-mb nuclear scattering cross sections, so that the dominant loss mechanism is liable to come from spallation-product nuclear collisions with the background residual gas. Note that typical ionization cross sections are 15 orders of magnitude larger than capture cross sections (for $Z_p = 1$, $Z_t = 1$), so that the lifetime against ionization is less than $10^{-4}$–$10^{-1}$ hours in $H_2$ gas. Circulating anything but fully stripped ions is not viable.

## V. CONCLUSIONS

At ultrarelativistic energies, all of the capture and ionization processes investigated in our earlier papers on 0.1- to 2-GeV/amu collisions assume simple asymptotic energy dependences, so that the relevant cross sections can be calculated simply using a few tables. We hope the formulas given in this paper will be of use to the design of future particle accelerators and perhaps have other applications.

## ACKNOWLEDGMENTS

This work was supported in part by the National Science Foundation Grant No. PHY-86-14650. One of us (U.B.) is supported by Deutscher Akademischer Austauschdienst (DAAD), Bonn, West Germany.

## APPENDIX: CROSS-SECTION CALCULATIONS

As an example of the use of Tables I–IV, we consider the calculation of the cross sections for capture and ionization by oxygen ions ($Z_p = 8$) with $\gamma = 100$ in $N_2$ ($Z_t = 7$). From Table I we find the value of 2.93 nb for $Z_p = 8$, hence from Eq. (1)

$$\sigma_{REC} = \frac{2.93 \times 10^{-9} \times 8^5 \times 7}{100} = 6.7 \times 10^{-6} \text{ b} . \quad \text{(A1)}$$

The units are per target atom and per bare projectile. For vacuum capture, Eq. (2) and Table I give

$$\sigma_{VAC} = 2.76 \times 10^{-12}(7^2+7)8^5 \ln\left[\frac{100}{6.83}\right] = 1.39 \times 10^{-5} \text{ b} . \quad \text{(A2)}$$

For NRC, Table II for $Z_p = 8$ and $Z_t = 7$ gives $9.09 \times 10^{-18}$ b, hence

$$\sigma_{NRC} = 9.09 \times 10^{-18} \frac{7^5 8^5}{100} = 5 \times 10^{-11} \text{ b} . \quad \text{(A3)}$$

The total capture cross section is therefore $2.06 \times 10^{-5}$ b.

For Coulomb and transverse ionization, Tables III and IV give

$$\sigma_{Coul} = 3.53 \times 10^4 (7/8)^2 = 2.7 \times 10^4 \text{ b} ,$$
$$\sigma_{trans} = 93.8(7/8)^2(2 \ln 100 - 1) = 589 \text{ b} . \quad \text{(A4)}$$

The total ionization cross section is therefore $2.75 \times 10^4$ b, and $R_{eq} = 7.46 \times 10^{-10}$.

The storage lifetime $\tau$ is given by

$$\tau^{-1} = n \sigma_{capt} c , \quad \text{(A5)}$$

where $n$ is the target atom density and $c$ is the speed of light. Inserting the total capture cross section, we obtain

$$\tau^{-1} = 2 \times 0.602 \times 10^{24} \times 2.06 \times 10^{-29} \text{ cm}^2 \times 10^{-8} \text{ torr} \times 3 \times 10^{10} \text{ cm/sec} \times 3600 \text{ sec/hr}/(22.4 \times 10^3 \text{ cm}^3 \times 760 \text{ torr}),$$
$$\tau = 6.3 \times 10^5 \text{ hours} . \quad \text{(A6)}$$

The factor of 2 comes from the two atoms in the $N_2$ molecule.

*Present address: Solid State Electronics Laboratory, Department of Electrical Engineering, Stanford University, Stanford, CA 94305.

†Present address: Institut für Theoretische Physik, Justus-Liebig-Universität, 6300 Giessen, West Germany.

[1]R. Anholt, Phys. Rev. A **31**, 3579 (1985) (paper II).

[2]W. E. Meyerhof, R. Anholt, J. Eichler, H. Gould, Ch. Munger, J. Alonso, P. Thieberger, and H. E. Wegner, Phys. Rev. A **32**, 3291 (1985) (paper III).

[3]R. Anholt, W. E. Meyerhof, H. Gould, Ch. Munger, J. Alonso, P. Thieberger, and H. E. Wegner, Phys. Rev. A **32**, 3302 (1985) (paper IV).

[4]R. Anholt, W. E. Meyerhof, X.-Y. Xu, H. Gould, B. Feinberg, R. J. McDonald, H. E. Wegner, and P. Thieberger, Phys. Rev. A **36**, 1586 (1987) (paper VIII).

[5]R. Anholt, Phys. Rev. A **19**, 1004 (1979).

[6]R. Anholt and J. Eichler, Phys. Rev. A **31**, 3505 (1985).

[7]J. Eichler, Phys. Rev. A **32**, 112 (1985).

[8]U. Becker, N. Grun, and W. Scheid, J. Phys. B **20**, 2075 (1987); U. Becker, J. Phys. B (to be published).

[9]C. A. Bertulani and G. Baur (unpublished).

[10]F. Sauter, Ann. Phys. (N.Y.) **9**, 217 (1931).

[11]R. H. Pratt, Phys. Rev. **117**, 1017 (1960).

[12]W. J. Humphries and B. L. Moisewitsch, J. Phys. B **17**, 2655 (1984).

[13]J. Eichler, Phys. Rev. A **35**, 3248 (1987).

[14]D. H. Jakubassa-Amundsen and P. A. Amundsen, Z. Phys. A **298**, 113 (1980).

[15]D. M. Davidovic, B. L. Moiseiwitsch, and P. H. Norrington, J. Phys. B **11**, 847 (1978).

[16]H. Gould, Lawrence Berkeley Laboratory Report No. LBL-18593, 1984 (unpublished).

[17]A Sommerfeld and A. W. Maue, Ann. Phys. **22**, 629 (1935); see also W. Furry, Phys. Rev. **46**, 391 (1934).

[18]G. S. Khandelwal, B. H. Choi, and E. Merzbacher, At. Data **1**, 102 (1969).

[19]B. H. Choi, E. Merzbacher, and G. S. Khandelwal, At. Data **5**, 291 (1973).

[20]J. H. McGuire, N. Stolterfoht, and P. R. Simony, Phys. Rev. A **24**, 97 (1981).